Research Article | Vol. 8, No. 2 | 1 Feb 2017 | BIOMEDICAL OPTICS EXPRESS 974
Biomedical Optics EXPRESS

In vivo imaging of hepatic hemodynamics and light scattering property during ischemia-reperfusion in rats based on spectrocolorimetry

SHARMIN AKTER,[1] SATOKO KAWAUCHI,[2] SHUNICHI SATO,[2] SUEFUMI AOSASA,[3] JUNJI YAMAMOTO,[3] AND IZUMI NISHIDATE[1,*]

[1]*Graduate School of Bio-Applications & Systems Engineering, Tokyo University of Agriculture and Technology, 2-24-16 Naka-cho, Koganei, Tokyo 184-8588, Japan*
[2]*Division of Biomedical Information Sciences, National Defense Medical College Research Institute, 3-2 Namiki, Tokorozawa, Saitama 359-8513, Japan*
[3]*Department of Surgery, National Defense Medical College, 3-2 Namiki, Tokorozawa, Saitama 359-8513, Japan*
[*]*inishi@cc.tuat.ac.jp*

Abstract: A red-green-blue camera-based imaging method is proposed for estimating spatial maps of concentrations of oxyhemoglobin (C_{HbO}), deoxyhemoglobin (C_{HbR}), total hemoglobin (C_{HbT}), tissue oxygen saturation (StO_2), and scattering power (b) in liver tissue. Hemodynamic responses to hepatic ischemia-reperfusion of *in vivo* rat liver tissues induced by portal triad occlusion were evaluated. Upon portal triad occlusion, this method yielded images of decreased C_{HbO}, C_{HbT}, StO_2, and b, and increased C_{HbR} followed by a progressive increase in C_{HbO} and StO_2 during reperfusion. Time courses of the changes in C_{HbO}, C_{HbR}, C_{HbT}, and StO_2 over different regions of interest (ROI_s) revealed that ischemia results in an abrupt significant ($P<0.05$) reduction in C_{HbO}, C_{HbT}, and StO_2 with a simultaneous increase in C_{HbR} compared to the baseline level, indicative of the hemodynamic responses during hepatic ischemia-reperfusion. Upon reperfusion, there was a gradual increase in C_{HbO} and StO_2, and decrease in C_{HbR}. The change in average scattering power b implies the presence of morphological alterations in the cellular and subcellular structures induced by ischemia or anoxia. This study shows the potential of monitoring spatiotemporal changes in hemodynamic parameters and morphological changes in studies of hepatic pathophysiology.

OCIS codes: (170.0170) Medical optics and biotechnology; (170.3880) Medical and biological imaging; (170.6510) Spectroscopy, tissue diagnostics; (170.3010) Image reconstruction techniques; (170.0110) Imaging systems.

References and links

1. K. Chun, J. Zhang, J. Biewer, D. Ferguson, and M. G. Clemens, "Microcirculatory failure determines lethal hepatocyte injury in ischemic/reperfused rat livers," Shock **1**(1), 3–9 (1994).
2. R. Cursio, P. Colosetti, M. C. Saint-Paul, S. Pagnotta, P. Gounon, A. Iannelli, P. Auberger, and J. Gugenheim, "Induction of different types of cell death after normothermic liver ischemia-reperfusion," Transplant. Proc. **42**(10), 3977–3980 (2010).
3. M. Goto, S. Kawano, H. Yoshihara, Y. Takei, T. Hijioka, H. Fukui, T. Matsunaga, M. Oshita, T. Kashiwagi, H. Fusamoto, T. Kamada, and N. Sato, "Hepatic tissue oxygenation as a predictive indicator of ischemia-reperfusion liver injury," Hepatology **15**(3), 432–437 (1992).
4. J. H. Pringle, "Notes on the arrest of hepatic hemorrhage due to trauma," Ann. Surg. **48**(4), 541–549 (1908).
5. J. R. Mourant, J. P. Freyer, A. H. Hielscher, A. A. Eick, D. Shen, and T. M. Johnson, "Mechanisms of light scattering from biological cells relevant to noninvasive optical-tissue diagnostics," Appl. Opt. **37**(16), 3586–3593 (1998).
6. D. Abookasis, C. C. Lay, M. S. Mathews, M. E. Linskey, R. D. Frostig, and B. J. Tromberg, "Imaging cortical absorption, scattering, and hemodynamic response during ischemic stroke using spatially modulated near-infrared illumination," J. Biomed. Opt. **14**(2), 024033 (2009).
7. X. Wang, B. W. Pogue, S. Jiang, X. Song, K. D. Paulsen, C. Kogel, S. P. Poplack, and W. A. Wells, "Approximation of Mie scattering parameters in near-infrared tomography of normal breast tissue in vivo," J. Biomed. Opt. **10**(5), 051704 (2005).

#280435 http://dx.doi.org/10.1364/BOE.8.000974
Journal © 2017 Received 8 Nov 2016; revised 11 Jan 2017; accepted 14 Jan 2017; published 19 Jan 2017

Biomedical Optics EXPRESS

8. J. R. Mourant, T. Fuselier, J. Boyer, T. M. Johnson, and I. J. Bigio, "Predictions and measurements of scattering and absorption over broad wavelength ranges in tissue phantoms," Appl. Opt. **36**(4), 949–957 (1997).
9. V. Tuchin, *Tissue Optics: Light scattering Methods and Instruments for Medical Diagnosis*, 2nd ed. (SPIE Press, Bellingham, Washington 2007).
10. B. I. Sykes, E. Penny, and I. F. Purchase, "Hepatocyte vacuolation and increased liver weight occurring in anoxic rats," Toxicol. Appl. Pharmacol. **36**(1), 31–39 (1976).
11. O. A. Trowell, "The experimental production of watery vacuolation of the liver," J. Physiol. **105**(3), 268–297 (1946).
12. S. Akter, S. Maejima, S. Kawauchi, S. Sato, A. Hinoki, S. Aosasa, J. Yamamoto, and I. Nishidate, "Evaluation of light scattering and absorption properties of in vivo rat liver using a single-reflectance fiber probe during preischemia, ischemia-reperfusion, and postmortem," J. Biomed. Opt. **20**(7), 076010 (2015).
13. M. Kretzschmar, A. Krüger, W. Schirrmeister, A. Krüger, and W. Schirrmeister, "Hepatic ischemia-reperfusion syndrome after partial liver resection (LR): hepatic venous oxygen saturation, enzyme pattern, reduced and oxidized glutathione, procalcitonin and interleukin-6," Exp. Toxicol. Pathol. **54**(5-6), 423–431 (2003).
14. S. Marubayashi, M. Takenaka, K. Dohi, H. Ezaki, and T. Kawasaki, "Adenine nucleotide metabolism during hepatic ischemia and subsequent blood reflow periods and its relation to organ viability," Transplantation **30**(4), 294–296 (1980).
15. W. Kamiike, M. Nakahara, K. Nakao, M. Koseki, T. Nishida, Y. Kawashima, F. Watanabe, and K. Tagawa, "Correlation between cellular ATP level and bile excretion in the rat liver," Transplantation **39**(1), 50–55 (1985).
16. J. J. Lemasters, H. Bunzendahl, and R. G. Thurman, "Reperfusion injury to donor livers stored for transplantation," Liver Transpl. Surg. **1**(2), 124–138 (1995).
17. J. W. Kupiec-Weglinski and R. W. Busuttil, "Ischemia and reperfusion injury in liver transplantation," Transplant. Proc. **37**(4), 1653–1656 (2005).
18. A. E. El-Desoky, D. T. Delpy, B. R. Davidson, and A. M. Seifalian, "Assessment of hepatic ischaemia reperfusion injury by measuring intracellular tissue oxygenation using near infrared spectroscopy," Liver **21**(1), 37–44 (2001).
19. C. Sturesson, D. M. Milstein, I. C. Post, A. M. Maas, and T. M. van Gulik, "Laser speckle contrast imaging for assessment of liver microcirculation," Microvasc. Res. **87**, 34–40 (2013).
20. C. H. Li, H. D. Wang, J. J. Hu, X. L. Ge, K. Pan, A. Q. Zhang, and J. H. Dong, "The monitoring of microvascular liver blood flow changes during ischemia and reperfusion using laser speckle contrast imaging," Microvasc. Res. **94**, 28–35 (2014).
21. H. Wang, X. Liang, Y. H. Mohammed, J. A. Thomas, K. R. Bridle, C. A. Thorling, J. E. Grice, Z. P. Xu, X. Liu, D. H. Crawford, and M. S. Roberts, "Real-time histology in liver disease using multiphoton microscopy with fluorescence lifetime imaging," Biomed. Opt. Express **6**(3), 780–792 (2015).
22. J. Yan, Y. Kang, S. Xu, L. L. S. Ong, S. Zhuo, R. M. Bunte, N. Chen, H. H. Asada, P. T. C. So, I. R. Wanless, and H. Yu, "In vivo label-free quantification of liver microcirculation using dual-modality microscopy," J. Biomed. Opt. **19**(11), 116006 (2014).
23. H. H. Lu, Y. M. Wu, W. T. Chang, T. Luo, Y. C. Yang, H. D. Cho, and I. Liau, "Molecular imaging of ischemia and reperfusion in vivo with mitochondrial autofluorescence," Anal. Chem. **86**(10), 5024–5031 (2014).
24. S. Akter, T. Tanabe, S. Maejima, S. Kawauchi, S. Sato, A. Hinoki, S. Aosasa, J. Yamamoto, and I. Nishidate, "In vivo estimation of optical properties of rat liver using single-reflectance fiber probe during ischemia and reperfusion," Opt. Rev. **22**(6), 1–6 (2015).
25. I. Nishidate, N. Tanaka, T. Kawase, T. Maeda, T. Yuasa, Y. Aizu, T. Yuasa, and K. Niizeki, "Noninvasive imaging of human skin hemodynamics using a digital red-green-blue camera," J. Biomed. Opt. **16**(8), 086012 (2011).
26. K. Yoshida, I. Nishidate, T. Ishizuka, S. Kawauchi, S. Sato, and M. Sato, "Multispectral imaging of absorption and scattering properties of in vivo exposed rat brain using a digital red-green-blue camera," J. Biomed. Opt. **20**(5), 051026 (2015).
27. I. Nishidate, T. Ishizuka, A. Mustari, K. Yoshida, S. Kawauchi, S. Sato, and M. Sato, "Evaluation of cerebral hemodynamics and tissue morphology of in vivo rat brain using spectral diffuse reflectance imaging," Appl. Spectrosc. **2016**, 03702816657569 (2016).
28. L. Wang, S. L. Jacques, and L. Zheng, "MCML--Monte Carlo modeling of light transport in multi-layered tissues," Comput. Methods Programs Biomed. **47**(2), 131–146 (1995).
29. V. Tuchin, *Tissue Optics: Light Scattering Methods and Instruments for Medical Diagnosis*, 2nd ed., (SPIE Press, Bellingham, WA 2007).
30. S. A. Prahl, "Tabulated molar extinction coefficient for hemoglobin in water," http://omlc.org/spectra/hemoglobin/summery.html (1991).
31. T. Kitai, A. Tanaka, A. Tokuka, K. Tanaka, Y. Yamaoka, K. Ozawa, and K. Hirao, "Quantitative detection of hemoglobin saturation in the liver with near-infrared spectroscopy," Hepatology **18**(4), 926–936 (1993).
32. A. Koo, I. Y. Liang, and K. K. Cheng, "The terminal hepatic microcirculation in the rat," Q. J. Exp. Physiol. Cogn. Med. Sci. **60**(4), 261–266 (1975).
33. T. Kondo, T. Todoroki, T. Hirano, F. W. Schildberg, and K. Messmer, "Impact of ischemia-reperfusion injury on dimensional changes of hepatic microvessels," Res. Exp. Med. (Berl.) **198**(2), 63–72 (1998).
34. M. D. Menger, M. Rücker, and B. Vollmar, "Capillary dysfunction in striated muscle ischemia/reperfusion: on the mechanisms of capillary "no-reflow"," Shock **8**(1), 2–7 (1997).

Biomedical Optics EXPRESS

35. B. Vollmar, J. Glasz, R. Leiderer, S. Post, and M. D. Menger, "Hepatic microcirculatory perfusion failure is a determinant of liver dysfunction in warm ischemia-reperfusion," Am. J. Pathol. **145**(6), 1421–1431 (1994).
36. F. J. Burczynski, B. A. Luxon, and R. A. Weisiger, "Intrahepatic blood flow distribution in the perfused rat liver: effect of hepatic artery perfusion," Am. J. Physiol. **271**(4 Pt 1), G561–G567 (1996).
37. M. N. Tawadrous, X. Y. Zhang, and A. M. Wheatley, "Microvascular origin of laser-Doppler flux signal from the surface of normal and injured liver of the rat," Microvasc. Res. **62**(3), 355–365 (2001).
38. M. G. Clemens, P. F. McDonagh, I. H. Chaudry, and A. E. Baue, "Hepatic microcirculatory failure after ischemia and reperfusion: improvement with ATP-MgCl2 treatment," Am. J. Physiol. **248**(6 Pt 2), H804–H811 (1985).
39. R. M. Zwacka, Y. Zhang, W. Zhou, J. Halldorson, and J. F. Engelhardt, "Ischemia/reperfusion injury in the liver of BALB/c mice activates AP-1 and nuclear factor kappaB independently of IkappaB degradation," Hepatology **28**(4), 1022–1030 (1998).
40. N. Sato, N. Hayashi, S. Kawano, T. Kamada, and H. Abe, "Hepatic hemodynamics in patients with chronic hepatitis or cirrhosis as assessed by organ-reflectance spectrophotometry," Gastroenterology **84**(3), 611–616 (1983).
41. M. Ohkawa, I. H. Chaudry, M. G. Clemens, and A. E. Baue, "ATP-MgCl2 produces sustained improvement in hepatic mitochondrial function and blood flow after hepatic ischemia," J. Surg. Res. **37**(3), 226–234 (1984).
42. J. C. Caldwell-Kenkel, R. T. Currin, Y. Tanaka, R. G. Thurman, and J. J. Lemasters, "Reperfusion injury to endothelial cells following cold ischemic storage of rat livers," Hepatology **10**(3), 292–299 (1989).
43. A. Leaf, "Cell swelling. A factor in ischemic tissue injury," Circulation **48**(3), 455–458 (1973).
44. M. D. Menger, S. Pelikan, D. Steiner, and K. Messmer, "Microvascular ischemia-reperfusion injury in striated muscle: significance of "reflow paradox"," Am. J. Physiol. **263**(6 Pt 2), H1901–H1906 (1992).
45. H. Jaeschke and J. J. Lemasters, "Apoptosis versus oncotic necrosis in hepatic ischemia/reperfusion injury," Gastroenterology **125**(4), 1246–1257 (2003).
46. G. Oldani, M. Maestri, A. Gaspari, E. Lillo, G. Angelastri, L. M. Lenti, J. Rademacher, M. Alessiani, and P. Dionigi, "A novel technique for rat liver transplantation using Quick Linker system: a preliminary result," J. Surg. Res. **149**(2), 303–309 (2008).
47. L. Yao, C. Li, X. Ge, H. Wang, K. Xu, A. Zhang, and J. Dong, "Establishment of a rat model of portal vein ligation combined with in situ splitting," PLoS One **9**(8), e105511 (2014).
48. J. C. Ramella-Roman, K. Lee, S. A. Prahl, and S. L. Jacques, "Design, testing, and clinical studies of a handheld polarized light camera," J. Biomed. Opt. **9**(6), 1305–1310 (2004).

1. Introduction

Ischemia and subsequent reperfusion of liver tissue may occur in a number of clinical settings, such as those associated with low-flow states, or temporary occlusion of the supplying blood vessels during liver transplantation, and to a large extent in liver resection surgery. Hepatic ischemia-reperfusion is characterized by circulatory derangement, including decreases in sinusoidal diameters and blood flow, increases in the heterogeneity of hepatic microvascular perfusion, and even total cessation of blood flow within individual sinusoids [1]. Therefore, ischemia-reperfusion damage to donor liver tissue is thought to be a vital component that may play a role in the decline of posttransplant graft function and ultimately rejection. In liver transplantation, normothermic ischemia-reperfusion causes up to 10% of early graft rejections [2]. Hepatocellular damage caused by ischemia-reperfusion correlates with the extent of microcirculatory reperfusion failure after portal-triad cross-clamping [3]. For liver transplantation, the hepatic pedicle is temporarily clamped (Pringle maneuver) [4] to restrict blood inflow and to reduce intraoperative blood loss, which results in deprivation of tissue oxygen and depletion of energy production, thereby shifting cellular metabolism to anaerobic pathways. The resulting hepatic ischemia, along with subsequent reperfusion, causes ischemia-reperfusion injury and structural changes in hepatic tissue of varying extents, which will also alter the scattering properties of light.

The spectra of reduced scattering coefficient $\mu_s'(\lambda)$ in biological soft tissues follow a power law function [5,6] that can be approximated in the following form:

$$\mu_s'(\lambda) = a\lambda^{-b}, \tag{1}$$

where a is the scattering amplitude and b is the scattering power, which are related to geometrical properties such as scatterer density [7] and size [8], respectively. It has been reported that a decrease or an increase in scattering power b produces an increase or decrease in scatterer size, respectively [8]. The reduced scattering coefficient spectrum $\mu_s'(\lambda)$ of

Biomedical Optics EXPRESS

biological tissues is considered to be the product of the combination of $\mu_s'(\lambda)$ for cellular and subcellular structures of different sizes [9]. The changes in scattering during ischemia are thought to originate from ischemia-induced changes in cellular and subcellular structures, whereas post-anoxia alterations indicate hepatocyte vacuolation [10–12]. Thus, it is important to measure the b to evaluate morphological changes in liver tissue resulting from ischemia, reperfusion and anoxia. Estimates of b can be used to evaluate the sizes of scatterers in liver tissue.

Hepatic ischemia-reperfusion results in a cascade of events leading to a number of cellular changes that evolve over time and space. Monitoring the spatio-temporal characteristics of changes in hemoglobin concentrations and tissue oxygen saturation is crucial for studying the pathophysiologic condition of liver tissue. Moreover, measurement of hepatic tissue oxygenation has been shown to correlate significantly with the microcirculatory derangement and hepatic dysfunction induced by ischemia-reperfusion. Reestablishment of blood flow to the liver tissue represents a vital requirement for recovery of cellular and organ function, which typically aggravates ischemia-induced tissue damage. Moreover, during reperfusion an additional insult is added to damage sustained during ischemia [13].

Several studies have reported that post-ischemic reperfusion is associated with inadequate energy supply, and a subsequent reduction of hepatic tissue oxygen saturation [3], impairment of mitochondrial adenosine triphosphate (ATP) regeneration [14], along with incomplete recovery of hepatocellular excretory function [15]. Hypoxic or ischemic damage to the hepatic sinusoidal endothelium is generally considered to be the first pathological change in the cascade of events resulting in ischemia-reperfusion injury during the manifestation of graft dysfunction [16]. Ischemia-reperfusion injury is closely related to an increase in the incidence of rapid decreases in tissue oxygen saturation StO_2, reduction of heme aa_3 in cytochrome c oxidase indicating mitochondrial dysfunction, and hepatocellular injury such as apoptosis, necrosis, and cell death [17]. On reentry of blood into the organ during reperfusion, there is an overproduction of toxic oxygen radicals followed by endothelial cell damage, causing disturbances in the microcirculation of liver tissue that lead to alterations in hepatic tissue oxygenation [3].

However, minimizing the detrimental effects of ischemia-reperfusion injury could increase the number of patients that successfully undergo transplantation. Maintenance of adequate hepatic blood flow and sufficient hepatic oxygenation is one of the most important factors in hepatic surgical success. As liver function depends greatly on hemodynamics and viability of liver tissue, measurements of concentrations of oxyhemoglobin (C_{HbO}), deoxyhemoglobin (C_{HbR}), total hemoglobin (C_{HbT}), and tissue oxygen saturation (StO_2) in hepatic tissue have been shown to correlate significantly with microcirculatory liver failure induced by ischemia-reperfusion injury [18]. One of the principal causes of hepatic ischemia-reperfusion injury is a biphasic phenomenon whereby cellular damage due to hypoxia and loss of biochemical stimulus is accentuated upon restoration of oxygen delivery and shear stress. Therefore, it is important to measure the hemodynamic response to ischemia-reperfusion such as changes in C_{HbO}, C_{HbR}, C_{HbT}, and StO_2.

Laser speckle contrast imaging (LSCI) and intravital auto-fluorescence imaging have been used to monitor hepatic ischemia-reperfusion processes. LSCI has been used to assess the microvascular blood flow changes during hepatic ischemia-reperfusion [19,20]. A multi-photon microscopy with fluorescence lifetime imaging has been investigated to visualize and quantify the cellular morphology and microenvironment during hepatic ischemia-reperfusion [21]. A label-free imaging method that combines wide-field fluorescence microscopy and LSCI has been investigated to assess microvascular features of liver fibrosis induced by bile-duct ligation [22]. An intravital imaging technique with auto-fluorescence of mitochondrial flavins has been proposed to evaluate the pathophysiology of liver during ischemia-reperfusion [23].

Biomedical Optics EXPRESS

In our previous studies we used reflectance fiber probe based diffuse reflectance spectroscopy (DRS) to evaluate the optical properties (such as reduced scattering coefficient (μ_s'), absorption coefficient (μ_a), StO_2 and the oxidation of heme aa_3 in CcO) of *in vivo* liver tissue during ischemia and reperfusion evoked by portal triad occlusion [12,24]. The reflectance fiber probe-based spectroscopic technique provides spatially averaged information of the optical properties of biological tissues obtained from the measurement point. Optical imaging with a digital red-green-blue (RGB) color camera is a useful tool for extending DRS to spatial mapping of chromophore concentrations as well as StO_2 of *in vivo* biological tissues. Diffuse reflectance spectrum of *in vivo* liver reveals the optical absorption spectra of chromophores, such as oxyhemoglobin, deoxyhemoglobin and cytochrome c oxidase, which depends on the chromophore concentrations in hepatic tissue. Since hemoglobin is the predominant absorber in liver tissue, the severity of liver ischemia-reperfusion can be reliably assessed by measuring changes in C_{HbO}, C_{HbR}, C_{HbT}, and StO_2. Accordingly, we hypothesized that ischemia-reperfusion driven changes in chromophore concentrations and tissue oxygen saturation are associated with spatial inhomogeneity in the perfusion of liver lobules that ultimately alters the hemodynamics in liver tissue. The present study was performed to assess this hypothesis through spatial mappings of C_{HbO}, C_{HbR}, C_{HbT}, StO_2, and b using an RGB imaging system. The ability of RGB color imaging to assess the hemodynamic responses and tissue morphology following hepatic ischemia-reperfusion would provide important diagnostic information to the extent of ischemia-reperfusion injury resulting from liver transplantation or resection surgery.

The technique of diffuse reflectance imaging introduced by Nishidate *et al*. [25–27] can provide insight into alterations in rat liver hemodynamics and tissue morphology resulting from hepatic ischemia-reperfusion. Imaging with a digital RGB camera is a widely used technique for the non-invasive characterization of biological tissues where contrast is obtained from the absorption of light by hemoglobin in blood. This can be achieved using a digital RGB color camera and a white light source, which is very simple to implement [25, 26]. Moreover, application of this technique is straightforward in specific clinical settings and can be implemented with relatively inexpensive instrumentation. Therefore, a simple method that provides sequential spatially resolved images of C_{HbO}, C_{HbR}, C_{HbT}, StO_2, and b would aid in experimental studies of hepatic hemodynamics and tissue morphology involving ischemia-reperfusion. The RGB imaging technique has been used to image hemodynamics indices of C_{HbO}, C_{HbR}, C_{HbT}, and StO_2 for *in vivo* human skin [25]. In this article, this approach is modified and extended to imaging for both hemodynamics and the light scattering property of *in vivo* exposed liver tissues during pathophysiologic events, such as hepatic inflow occlusion and subsequent reperfusion. Therefore, we propose a method to visualize the spatial maps of C_{HbO}, C_{HbR}, C_{HbT}, StO_2, and b in the liver tissue using a digital RGB image.

2. Principle

The responses of RGB channels (I_{R}, I_{G}, and I_{B}) in each pixel of the liver tissue color image acquired by a digital RGB camera can be expressed as

$$\begin{bmatrix} I_{\mathrm{R}} \\ I_{\mathrm{G}} \\ I_{\mathrm{B}} \end{bmatrix} = \mathbf{L_1} \begin{bmatrix} X \\ Y \\ Z \end{bmatrix}, \tag{2}$$

where $\mathbf{L_1}$ is a transposition matrix to convert the tristimulus values in the Commission Internationale de l' Éclairage XYZ (CIEXYZ) color system X, Y, and Z to corresponding responses of I_{R}, I_{G}, and I_{B}, and $[\cdots]^T$ represents transposition of a vector. The tristimulus values X, Y, and Z in the above equation are defined as

$$X = \kappa \sum \mathrm{E}(\lambda)\bar{x}(\lambda)\Theta(\lambda), \tag{3}$$

Biomedical Optics EXPRESS

$$Y = \kappa \sum \mathrm{E}(\lambda)\bar{y}(\lambda)\Theta(\lambda), \tag{4}$$

$$Z = \kappa \sum \mathrm{E}(\lambda)\bar{z}(\lambda)\Theta(\lambda), \tag{5}$$

where λ, $E(\lambda)$, and $\Theta(\lambda)$ are the wavelengths, the spectral distribution of the illuminant, and the diffuse reflectance spectrum of liver tissue, respectively, whereas $\bar{x}(\lambda)$, $\bar{y}(\lambda)$, and $\bar{z}(\lambda)$ are color matching functions in the CIEXYZ color system. The values of constant κ that result in Y being equal to 100 for the perfect diffuser is given by

$$\kappa = \frac{100}{\sum \mathrm{E}(\lambda)\bar{y}(\lambda)}. \tag{6}$$

In Eqs. (3)-(5), the summation can be carried out using data at 10 nm intervals, from 400 to 700 nm. Assuming a single layered liver tissue contains oxyhemoglobin and deoxyhemoglobin, the diffuse reflectance of liver tissue Θ can be expressed as

$$\Theta = \frac{I_{\mathrm{d}}}{I_{\mathrm{i}}} = \int_0^\infty P(\mu_s', l)\exp[-(\mu_{a,\mathrm{HbO}} + \mu_{a,\mathrm{HbR}})l]dl, \tag{7}$$

where I_{d} and I_{i} are the detected and incident light intensities respectively, $P(\mu_s', l)$ is the path length probability function that depends on the scattering properties as well as on the geometry of the measurements, μ_s', μ_a, and l are the scattering coefficient, absorption coefficient, and the photon path length, respectively. In addition, the subscripts HbO and HbR indicate the oxygenated hemoglobin and deoxygenated hemoglobin, respectively. The absorption coefficient μ_a of each chromophore can be expressed as the product of its concentration C and the extinction coefficient ε, and can be defined as

$$\mu_a = C \times \varepsilon. \tag{8}$$

Therefore, the responses of I_{R}, I_{G}, and I_{B} can be expressed as a function of concentration of oxyhemoglobin (C_{HbO}) and deoxyhemoglobin (C_{HbR}).

Figure 1 shows a flowchart describing the estimation process using the proposed method. First, the responses of the RGB channels I_{R}, I_{G}, and I_{B} in each pixel of the image are transformed into XYZ-values by a matrix $\mathbf{N_1}$ as

$$\begin{bmatrix} X \\ Y \\ Z \end{bmatrix} = \mathbf{N_1} \begin{bmatrix} I_{\mathrm{R}} \\ I_{\mathrm{G}} \\ I_{\mathrm{B}} \end{bmatrix}. \tag{9}$$

We determined the matrix $\mathbf{N_1}$ based on measurements of a standard color chart (Color Checker, X-Rite Incorporated, Michigan, USA) that has 24 color chips and is supplied with data giving the CIEXYZ values for each chip under specific illuminations and corresponding reflectance spectra. The values of X, Y, and Z are then transformed into C_{HbO}, C_{HbR}, and b by matrix $\mathbf{N_2}$. It is difficult to determine the matrix $\mathbf{N_2}$ based on $\mathbf{L_1}$ and Eqs. (3)-(7) because $P(\mu_s', l)$ and l for each layer are usually unknown. We calculated 450 diffuse reflectance spectra $\Theta(\lambda)$ in a wavelength range from 400 to 700 nm at intervals of 10 nm by MCS for light transport [28] in skin tissue. The simulation model used here consisted of a single layer of liver tissue, in which $\mu_a(\lambda)$ and $\mu_s'(\lambda)$ are homogeneously distributed. The absorption coefficients $\mu_a(\lambda)$ converted from the concentrations C_{HbO} and C_{HbR} and the reduced scattering coefficient $\mu_s'(\lambda)$ deduced by the scattering amplitude a and the scattering power b were provided as inputs to the simulation, whereas the diffuse reflectance spectrum $\Theta(\lambda)$ was derived as output. The five different values of 60,258, 90,387, 120,516, 150,645, and 180,774 cm^{-1} were calculated by multiplying the typical value [29] of a by 0.5, 0.75, 1.0, 1.25, and

Biomedical Optics EXPRESS

1.5, respectively, whereas the five values of 1.24, 1.31, 1.38, 1.45, and 1.52 were calculated by multiplying the typical value [29] of b by 0.5, 0.75, 1.0, 1.25, and 1.5, respectively. The reduced scattering coefficients $\mu_s'(\lambda)$ of the liver tissue with the 25 different values were derived using Eq. (1). Using Eq. (1). The sum of the absorption coefficients of oxyhemoglobin and deoxyhemoglobin $\mu_{a,\mathrm{HbO}}(\lambda) + \mu_{a,\mathrm{HbR}}(\lambda) = \mu_{a,\mathrm{HbT}}(\lambda)$ for C_{HbT} = 5, 10, and 20% was used as input to the liver tissue in the simulation. The absorption coefficients of blood having a 44% hematocrit with 150 g/L of hemoglobin [30] were assumed to be equivalent to that of the dermis for the case in which C_{HbT} = 100%. Tissue oxygen saturation StO_2 was determined by $C_{\mathrm{HbO}}/C_{\mathrm{HbT}}$, and values of 0%, 20%, 40%, 60%, 80%, and 100% were used for the simulation. The diffuse-reflectance spectra $\Theta(\lambda)$ were simulated under the various combinations of C_{HbO}, C_{HbR}, a, and b, and then, used to calculate the XYZ-values based on Eqs. (3)-(6):

$$C_{\mathrm{HbO}} = \alpha_0 + \alpha_1 X + \alpha_2 Y + \alpha_3 Z, \tag{10}$$

$$C_{\mathrm{HbR}} = \beta_0 + \beta_1 X + \beta_2 Y + \beta_3 Z, \tag{11}$$

$$b = \gamma_0 + \gamma_1 X + \gamma_2 Y + \gamma_3 Z, \tag{12}$$

The regression coefficients α_i, β_i, and γ_i (i = 0, 1, 2, 3) reflect the contributions of the XYZ-values to C_{HbO}, C_{HbR}, and b, respectively, and were used as the elements of a 4 × 3 matrix $\mathbf{N_2}$ as

$$\mathbf{N}_2 = \begin{bmatrix} \alpha_0 & \alpha_1 & \alpha_2 & \alpha_3 \\ \beta_0 & \beta_1 & \beta_2 & \beta_3 \\ \gamma_0 & \gamma_1 & \gamma_2 & \gamma_3 \end{bmatrix}. \tag{13}$$

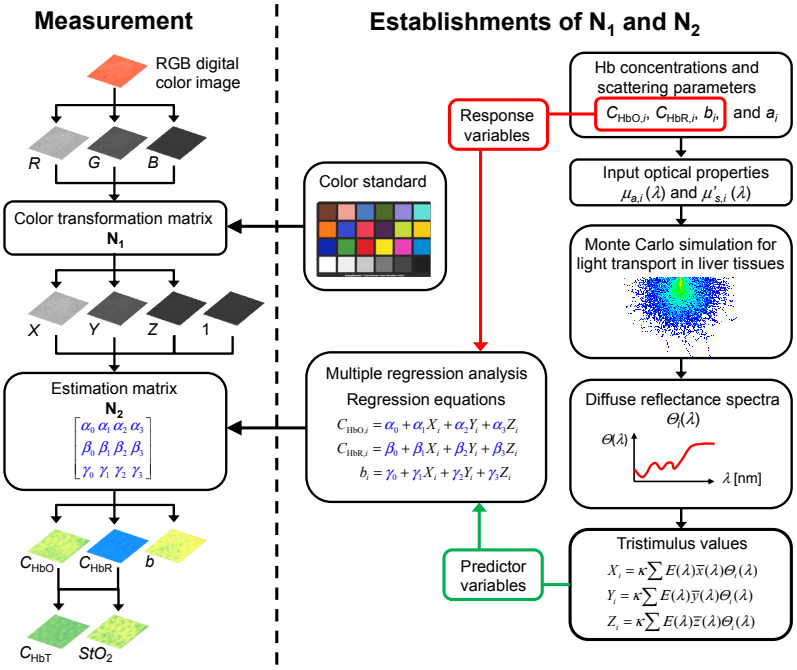

Fig. 1. Flowchart of the process for estimating the concentration of oxyhemoglobin C_{HbO}, deoxyhemoglobin C_{HbR}, total hemoglobin C_{HbT}, tissue oxygen saturation, StO_2, and scattering power b from the measured RGB-values.

Biomedical Optics EXPRESS

Transformation with $\mathbf{N_2}$ from the tristimulus values to chromophore concentrations is thus expressed as

$$\begin{bmatrix} C_{\mathrm{HbO}} \\ C_{\mathrm{HbR}} \\ b \end{bmatrix} = \mathbf{N}_2 \begin{bmatrix} 1 \\ X \\ Y \\ Z \end{bmatrix}. \tag{14}$$

Once we determine the matrices $\mathbf{N_1}$ and $\mathbf{N_2}$, images of C_{HbO}, C_{HbR} and b are reconstructed without the MCS. The total hemoglobin concentration image is simply calculated as $C_{\mathrm{HbT}} = C_{\mathrm{HbO}} + C_{\mathrm{HbR}}$ and tissue oxygen saturation of hemoglobin as $StO_2\% = (C_{\mathrm{HbO}}/C_{\mathrm{HbT}}) \times 100$.

3. Materials and methods

3.1 Measurement apparatus

The instrument developed for the RGB imaging system is illustrated in Fig. 2. A white-light emitting diode (LED) (LA-HDF60, Hayashi Watch Works Co., Ltd., Tokyo, Japan) illuminated the surface of the exposed rat liver tissue via a light guide and a ring-shaped illuminator with a polarizer. The light source covered a range from 400 nm to 780 nm. Diffusely reflected light, which contains information of liver tissue optical properties, was received by a 24-bit RGB CCD camera (DFK-21BF618.H Imaging source LLC, Charlotte, NC, USA) via an analyzer and a camera lens to acquire RGB images of 640 × 480 pixels. The ring shaped polarizer and analyzer were placed in a crossed Nicols alignment in order to reduce specular reflection of light from the liver surface. A standard white diffuser with 99%

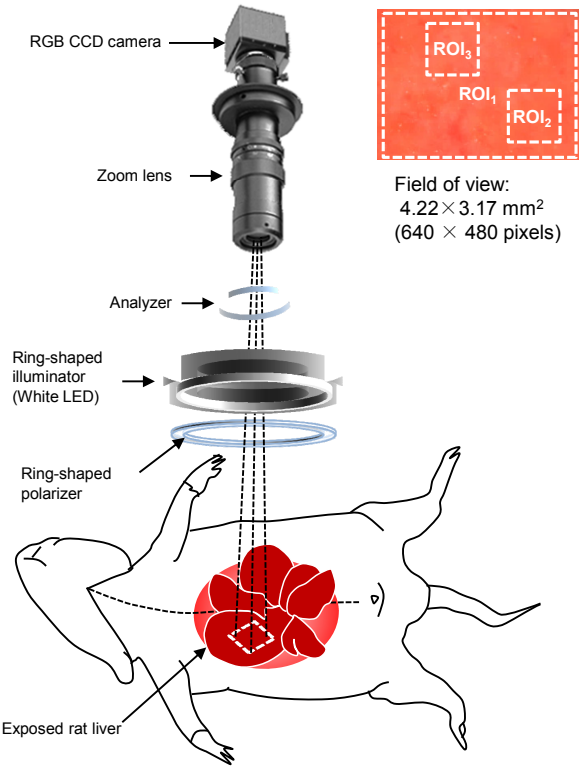

Fig. 2. Schematic illustration of setup for RGB imaging of hepatic hemodynamics. A white LED is used to illuminate the exposed rat liver, which is imaged using an RGB CCD camera. The computer acquires raw RGB images.

Biomedical Optics EXPRESS

reflectance (SRS-99-020, Labsphere Incorporated, New Hampshire, USA) was used to regulate the white balance of the camera, to correct instrument-to-instrument differences in output of the camera, and to correct the spatial nonuniformity of illumination. The field of view of the imaging system was calculated to be 4.22 mm × 3.17 mm from the measurement of the 1951 USAF resolution test chart. The number of pixel columns (width) was 640. The lateral pixel resolution of the images was estimated to be 4.22/640 = 0.0066 mm. The RGB images were then used to estimate the images of C_{HbO}, C_{HbR}, C_{HbT}, StO_2, and b according to the process described above.

3.2 Experiments

Male Wister rats (n = 5) weighing from 300 to 474 g were used for the experiment. All experimental procedures were conducted according to the protocols approved by the Animal Care Committee of Tokyo University of Agriculture and Technology. Anesthesia of rats was performed with α-chloralose (50 mg/kg) and urethane (600 mg/kg) by intraperitoneal injection. The rat liver ischemic model is depicted in Fig. 3. On laparotomy, the ligamentous attachments from the liver to the diaphragm and abdominal wall were dissected in order to mobilize the liver lobes. Hepatic ischemia was induced by clamping the portal triad (the hepatic artery, the portal vein, and the bile duct) supplying the median lobes and left lateral lobe with no occlusion of caudate lobe. A 10-minute ischemic period was followed by reperfusion for a period of 120 minutes. After 120 minutes of reperfusion, an anoxic condition was produced by nitrogen breathing. The liver surface was moistened with saline and covered with cover glass to prevent evaporation and the influence of the ambient air, and to reduce the surface reflection. Imaging was started before induction of ischemia to record baseline values and continued during ischemia, reperfusion and post mortem. Measurements of RGB color images were performed every 5 sec for a total of 160 min: oxygen breathing for 5 min, normal air breathing for 5 min, ischemia for 10 min, reperfusion for 120 min, and nitrogen breathing for 20 min.

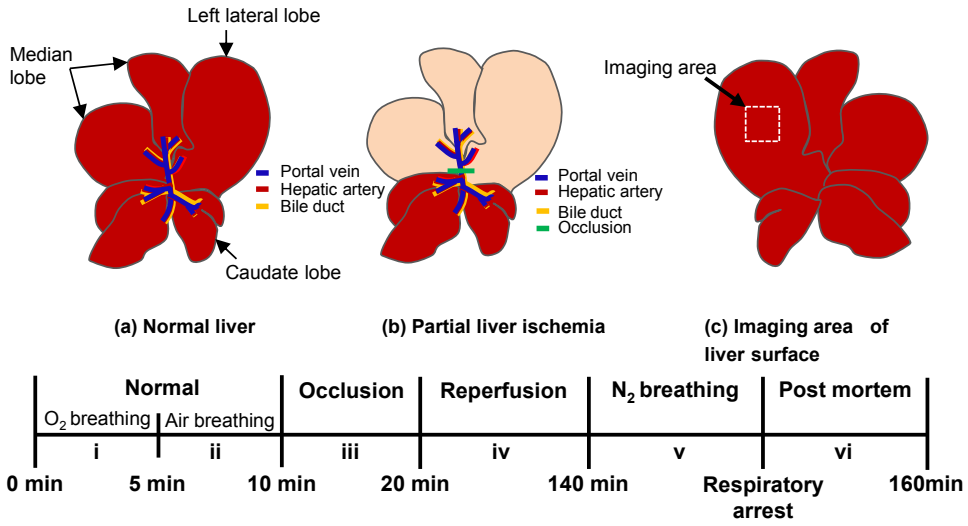

Fig. 3. Illustration of the (a) ventral surface of normal rat liver in which the left lateral and median lobes have been retracted to expose the portal vein (blue), hepatic artery (red), and common bile duct (yellow). (b) Cross-clamping of portal triad (green) induces ischemia to the left lateral and median lobes of the liver. (c) The dorsal surface of the liver lobe is shown as the imaging area.

To evaluate the magnitude of signal S before ischemia, during ischemia, reperfusion, nitrogen breathing, and post mortem, the relative change in the signal was calculated based on

Biomedical Optics EXPRESS

time series data. The signal measured at the normal condition (the end of the period of air-breathing) was used as a control S_c, which was subtracted from each of the subsequent signals S in the series. Each subtracted value, which demonstrated the change in the signal, $S - S_c$, over time, was normalized by dividing $S - S_c$ by Sc. The relative change in the signal is expressed as $\Delta S = \{(S - S_c)/S_c\}$. The above calculation was applied to the time series of C_{HbO}, C_{HbR}, C_{HbT}, StO_2, and b.

3.3 Statistical considerations

Estimation of C_{HbO}, C_{HbR}, C_{HbT}, StO_2, and b in hepatic tissue was performed based on the process described above. Regions of interest of 640 × 480 pixels (ROI_1, entire image), 150 × 150 pixels (ROI_2, relatively homogeneous region of perfusion), and 150 × 150 pixels (ROI_3, relatively heterogeneous region of perfusion) were set in each image for the analysis of time courses in C_{HbO}, C_{HbR}, C_{HbT}, StO_2, and b. Data are expressed as mean ± SD. In order to compare whether the mean of estimated value at each experimental condition differ significantly from the aggregate mean across the experimental conditions, one-way repeated measures ANOVA with Bonfferoni's correction was performed through statistical analysis when comparing the relative change in the signal between the ends of oxygen breathing (period i), air-breathing (period ii), ischemia (period iii), reperfusion (period iv), nitrogen-breathing (period v), and post mortem (period vi). A P value of less than 0.05/4 was considered to be statistically significant.

4. Results

Figure 4 shows typical *in vivo* results obtained from liver tissue, including RGB images, C_{HbO}, C_{HbR}, C_{HbT}, StO_2, and b images before ischemia (oxygen breathing, air breathing), during ischemia, reperfusion, nitrogen breathing, and post-mortem respectively. C_{HbO}, C_{HbR}, C_{HbT}, and StO_2 of the normal liver tissue (oxygen breathing and air breathing state) revealed high levels of oxyhemoglobin and tissue oxygen saturation. The large increase in C_{HbR} and decreases in C_{HbO} and StO_2 typically observed in ischemia are consistent with the changes in time courses in StO_2 reported in our previous studies [12,24]. Successive images recorded at 5-min after the onset of reperfusion (t = 25-min) show the spatial changes in C_{HbO} and StO_2 that are indicated by a white arrow on the less perfused portion of the imaged area, which is accompanied with scattered hepatic lobular perfusion. Immediately after reperfusion, a slight increase in C_{HbO} and StO_2 are observed in the imaged area, possibly indicating the gradual compensation of hepatic blood flow. In addition, we observed changes in C_{HbO}, C_{HbR}, C_{HbT}, and StO_2 at 2-min and 5-min after onset of nitrogen breathing (t = 142-min and t = 145-min) and found a rapid increase in C_{HbR} and C_{HbT} in post-mortem liver tissue. The image of scattering power b acquired at 2-min after onset of nitrogen breathing demonstrated a lower value compared to the reperfusion phase, followed by a subsequent increase at 5-min after onset of nitrogen breathing (shown in Fig. 11) is indicative of changes in average size of scatterers induced by anoxia. The tendency of changes in C_{HbO}, C_{HbR}, C_{HbT}, StO_2, and b following ischemia, reperfusion and post-mortem shown in Fig. 4 were evident in all five rats.

Time courses of the changes in C_{HbO}, C_{HbR}, C_{HbT}, and StO_2 averaged over the samples and over the entire imaged area (region of interest, ROI_1), relatively homogeneous region (region of interest, ROI_2), and relatively heterogeneous region (region of interest, ROI_3) indicated in Fig. 2 during the period of pre-ischemia (oxygen breathing and air breathing), ischemia, reperfusion, nitrogen breathing, and post-mortem are plotted in Figs. 5, 6, and 7, respectively. The symbols i, ii, iii, iv, v, and vi in each figure indicate O_2-breathing, air-breathing, ischemia under air-breathing, reperfusion under air-breathing, N_2-breathing, and post-mortem, respectively. The relative change in concentrations of C_{HbO}, C_{HbR}, C_{HbT}, and StO_2 in ROI_1, ROI_2, and ROI_3 at the ends of each period are shown in Figs. 8, 9, and 10, respectively.

In this study oxyhemoglobin and deoxyhemoglobin concentrations have been used as indices of total hemoglobin concentration and tissue oxygenation. From the time series

Biomedical Optics EXPRESS

measurements we found that C_{HbO} and C_{HbR} decreased and increased respectively following the onset of ischemia, compared to the preischemic levels. Consequently, StO_2 decreased, thereby reflecting reduced blood flow and oxygen supply to the tissue. The average oxyhemoglobin concentration over each period in ROI_1 was calculated to be 8.67 ± 0.06 during oxygen breathing, 8.08 ± 0.19 during air breathing, 4.02 ± 1.07 during ischemia, 6.55 ± 0.92 during post-reperfusion, and 1.33 ± 1.41 at post-mortem.

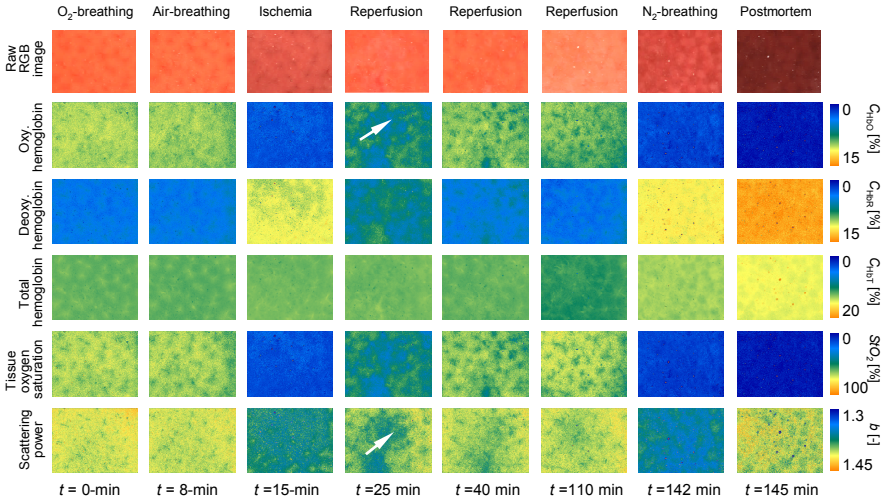

Fig. 4. Typical images of *in vivo* liver tissue at different measurement time points. Left to right: the first column of Fig. 4 shows images at t = 0-min (the beginning of measurement and 0-min after start of oxygen breathing), the second column shows images at t = 8-min (3-min after start of air breathing), the third column shows images at t = 15-min (5-min after the onset of ischemia), the fourth column shows images at t = 25-min (5-min after the onset of reperfusion), the fifth column shows images at t = 40-min (20-min after the onset of reperfusion), the sixth column shows images at t = 110-min (90-min after the onset of reperfusion), the seventh column shows images at t = 142-min (2-min after the onset of nitrogen breathing), and the eighth column shows images at t = 145-min (5-min after the onset of nitrogen breathing). Top to bottom: raw RGB images are shown in the top row with the corresponding C_{HbO}, C_{HbR}, C_{HbT}, StO_2 and scattering power b images reconstructed from the RGB images) under white light illumination shown in the following rows. Successive images recorded 5-min post-reperfusion show the spatial changes in C_{HbO} and StO_2 that are indicated by a white arrow on the less perfused portion of the imaged area, which is accompanied with scattered hepatic lobular perfusion.

Biomedical Optics EXPRESS

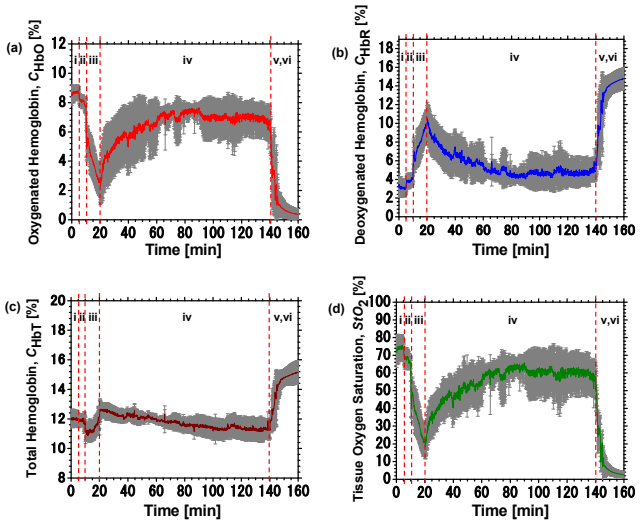

Fig. 5. Typical time courses of average chromophore concentration and tissue oxygen saturation averaged over the region of interest (ROI_1, entire image) for (a) oxygenated hemoglobin C_{HbO}, (b) deoxygenated hemoglobin C_{HbR}, (c) total hemoglobin C_{HbT}, and (d) tissue oxygen saturation StO_2. Data are expressed as mean ± SD (n = 5). The symbols i, ii, iii, iv, v, and vi in each figure indicate O_2-breathing, air-breathing, ischemia under air-breathing, reperfusion under air-breathing, N_2-breathing, and post-mortem, respectively.

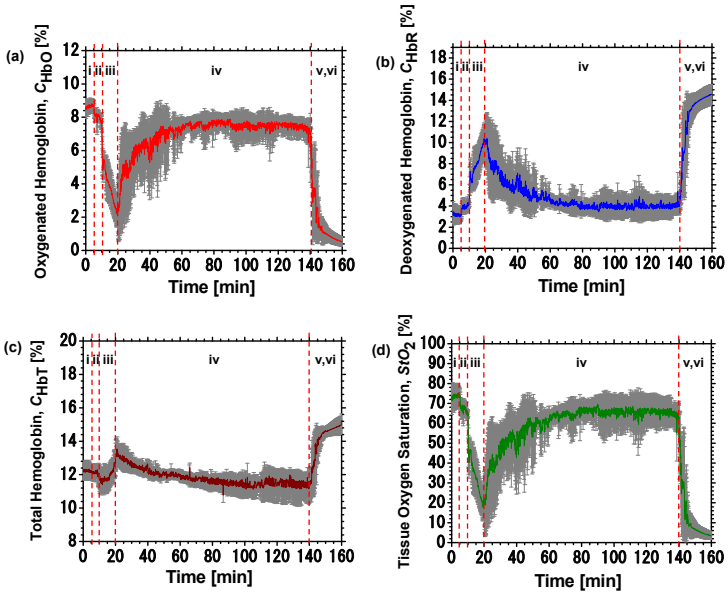

Fig. 6. Typical time courses of average chromophore concentration and tissue oxygen saturation averaged over the region of interest (ROI_2, relatively homogeneous region of perfusion) for (a) oxygenated hemoglobin C_{HbO}, (b) deoxygenated hemoglobin C_{HbR}, (c) total hemoglobin C_{HbT}, and (d) tissue oxygen saturation StO_2. Data are expressed as mean ± SD (n = 5). The symbols i, ii, iii, iv, v, and vi in each figure indicate O_2-breathing, air-breathing, ischemia under air-breathing, reperfusion under air-breathing, N_2-breathing, and post-mortem, respectively.

Biomedical Optics EXPRESS

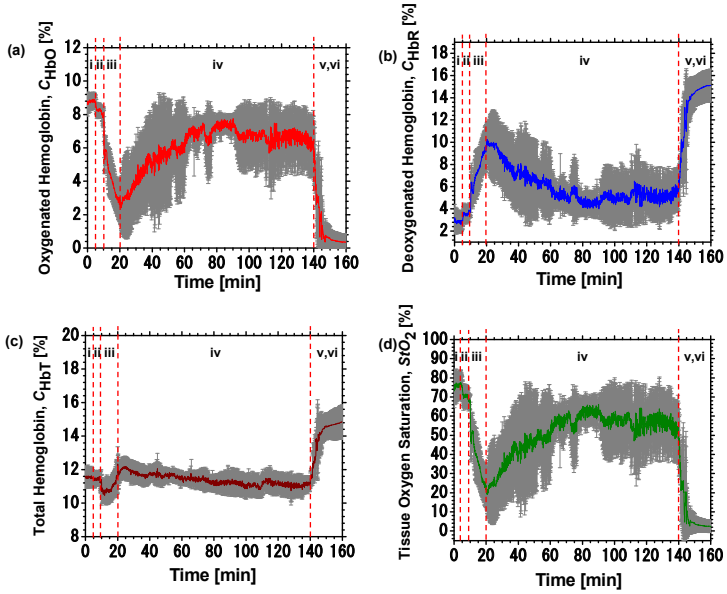

Fig. 7. Typical time courses of chromophore concentration and tissue oxygen saturation averaged over the region of interest (ROI_3, relatively heterogeneous region of perfusion) for (a) oxygenated hemoglobin C_{HbO}, (b) deoxygenated hemoglobin C_{HbR}, (c) total hemoglobin C_{HbT}, and (d) tissue oxygen saturation StO_2. Data are expressed as mean ± SD (n = 5). The symbols i, ii, iii, iv, v, and vi in each figure indicate O_2-breathing, air-breathing, ischemia under air-breathing, reperfusion under air-breathing, N_2-breathing, and post-mortem, respectively.

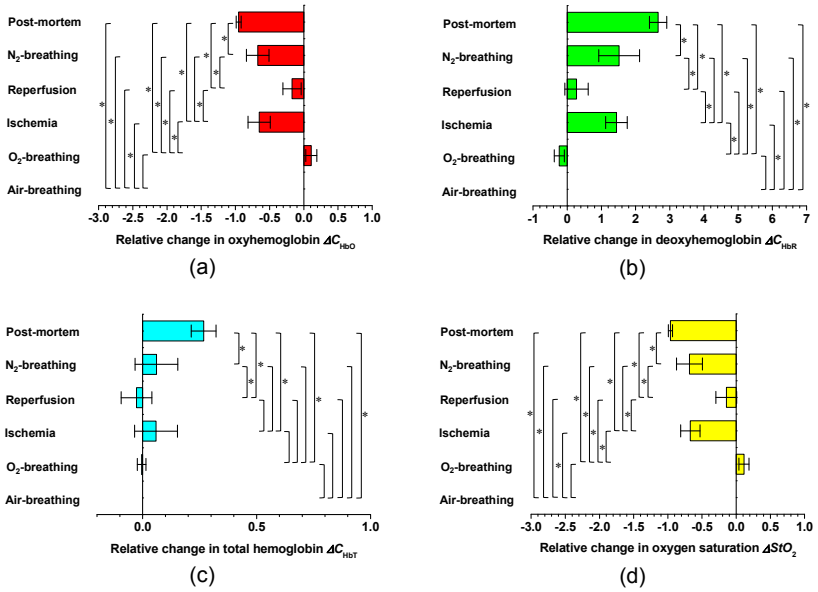

Fig. 8. The relative change in chromophore concentrations and tissue oxygen saturation (for ROI_1 shown in Fig. 2) at the ends of each period. (a) Oxygenated hemoglobin C_{HbO}, (b) deoxygenated hemoglobin C_{HbR}, (c) total hemoglobin C_{HbT}, and (d) tissue oxygen saturation StO_2. Data are expressed as mean ± SD (n = 5). *P < 0.05/4.

Biomedical Optics EXPRESS

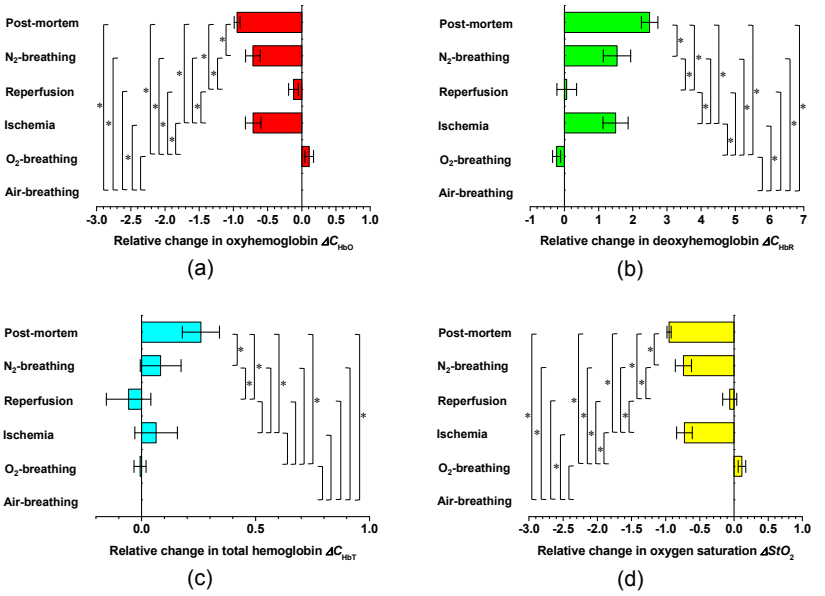

Fig. 9. The relative change in chromophore concentrations and tissue oxygen saturation (for ROI_2 shown in Fig. 2) at the ends of each period. (a) Oxygenated hemoglobin C_{HbO}, (b) deoxygenated hemoglobin C_{HbR}, (c) total hemoglobin C_{HbT}, and (d) tissue oxygen saturation StO_2. Data are expressed as mean ± SD ($n = 5$). *$P < 0.05/4$.

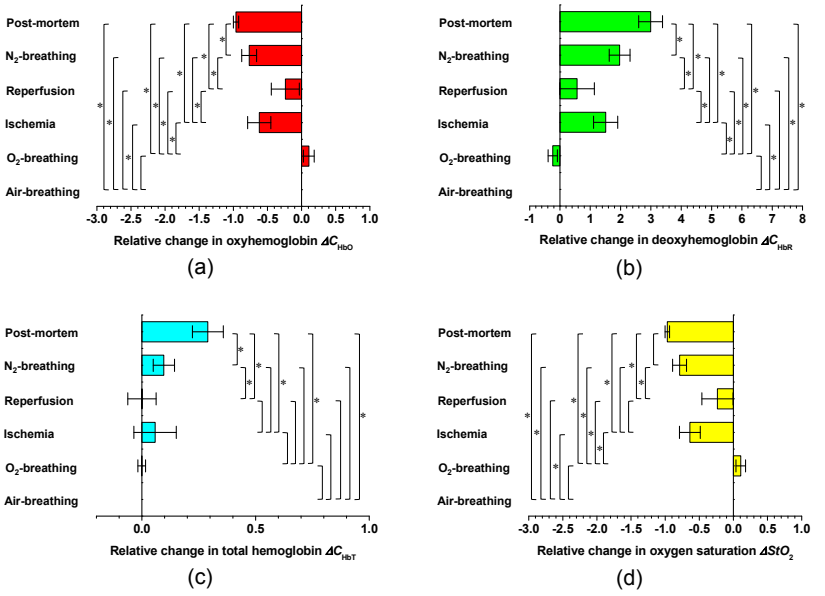

Fig. 10. The relative change in chromophore concentrations and tissue oxygen saturation (for ROI_3 shown in Fig. 2) at the ends of each period. (a) Oxygenated hemoglobin C_{HbO}, (b) deoxygenated hemoglobin C_{HbR}, (c) total hemoglobin C_{HbT}, and (d) tissue oxygen saturation StO_2. Data are expressed as mean ± SD ($n = 5$). *$P < 0.05/4$.

Ligation of hepatic pedicle of the median and left lateral lobes resulted in approximately 70% occlusion or ischemia of the liver [18], as indicated by a rapid decrease of hepatic StO_2 on the initiation of ischemia. Note that the decrease in C_{HbT} found at ischemia is possibly due

Biomedical Optics EXPRESS

to hepatic inflow occlusion and maintenance of outflow. Hepatic tissue oxygen saturation during oxygen breathing and air breathing (baseline) in ROI_1 were estimated to be 74.09 ± 0.70% and 68.12 ± 1.68%, respectively, which is comparable with or slightly greater than hepatic hemoglobin oxygen saturation (57.4% ± 2.5%; n = 7) in rabbits in room air [31]. Immediately after reflow of the portal triad, hepatic StO_2 showed a remarkably heterogeneous distribution with an average of 55.48 ± 8.72% in ROI_1 after 120 min of reperfusion. However, this did not return to baseline levels, possibly due to ischemia-reperfusion associated hepatic dysfunction.

Average StO_2 levels at the end of reperfusion in a relatively homogeneous region of interest (ROI_2) is recorded to be 60.52 ± 8.99%, which is relatively higher than that recorded from the entire imaged area (ROI_1). Conversely, hepatic tissue oxygen saturation in a relatively heterogeneous region of interest (ROI_3) showed lower reperfusion levels in comparison to that observed in the entire image (ROI_1) and the relatively homogeneous region of interest (ROI_2) in all five rats. The low hepatic StO_2 is possibly associated with sinusoidal length heterogeneity in rat liver, creating heterogeneity in hepatic blood flow [32]. In contrast, C_{HbR} calculated from ROI_1, ROI_2 and ROI_3 increased significantly during ischemia, probably due to tissue extraction of oxygen from hemoglobin, and slowly decreased with the time course of reperfusion. It is also interesting to note that immediately after respiratory arrest, C_{HbO} decreased and C_{HbR} increased, therefore the value of StO_2 dropped sharply compared to the reperfusion level. The average period between the onset of nitrogen breathing and the occurrence of respiratory arrest was recorded to be 144 ± 70.92 sec. C_{HbT} started to increase after the onset of nitrogen breathing and reached a maximum level immediately after respiratory arrest, which may be associated with high venous or intrahepatic blood pressure during the first few minutes of asphyxia and may persist for hours after death [11]. Time courses of C_{HbO}, C_{HbR}, C_{HbT}, and StO_2 over the ROI_s (depicted in Figs. 5, 6, and 7) revealed that the hemodynamic response of liver tissue associated with ischemia-reperfusion is characterized by a significant decrease in C_{HbO} and StO_2 at the onset of ischemia, compared to pre-ischemic levels. Additionally, subsequent reperfusion resulted in gradual increases in C_{HbO} and StO_2 with a simultaneous decrease in C_{HbR} compared to ischemic levels, which are consistent with the hemodynamic responses of hepatic ischemia-reperfusion.

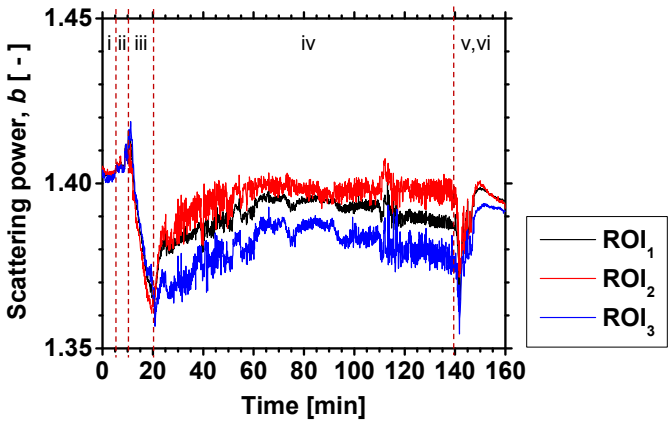

Fig. 11. Typical time course of scattering power b averaged over the regions of interest (ROI_1, entire image; ROI_2, relatively homogeneous region of perfusion; ROI_3, relatively heterogeneous region of perfusion). Data are expressed as mean ± SD (n = 5). The symbols i, ii, iii, iv, v, and vi in each figure indicate O_2-breathing, air-breathing, ischemia under air-breathing, reperfusion under air-breathing, N_2-breathing, and post-mortem, respectively.

Biomedical Optics EXPRESS

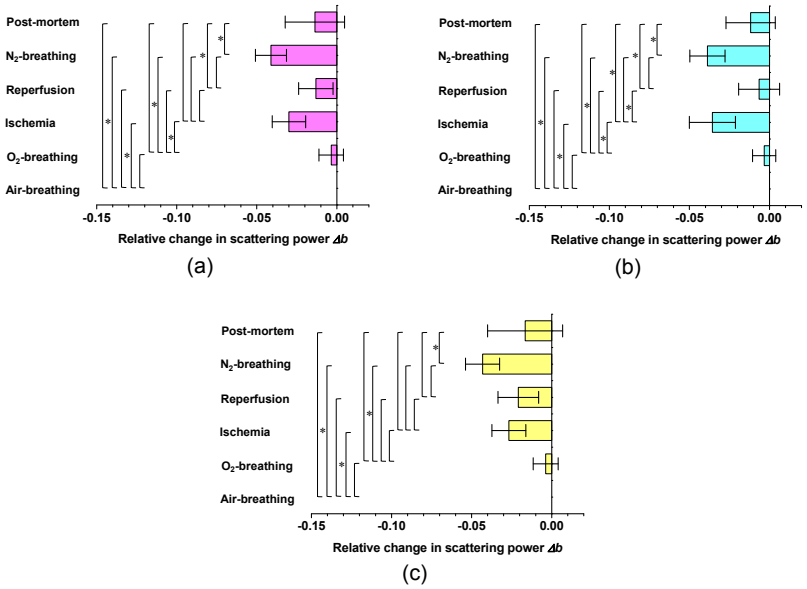

Fig. 12. The relative change in scattering power b at the ends of each period. (a) Entire imaged area (ROI_1), (b) relatively homogeneous region (ROI_2), and (c) relatively heterogeneous region (ROI_3). Data are expressed as mean ± SD (n = 5). *P < 0.05/4.

Changes in the average b over time for the ROIs shown in Fig. 4 are plotted in Fig. 11. Mean b for each ROI was significantly decreased during ischemia, which can be explained by an increase in the average size of scatterers. The average value of b at reperfusion obtained from ROI_1 is comparatively higher than that recorded from the relatively heterogeneous ROI_3 (Fig. 12). The maximum level of b was recorded from the relatively homogeneous region of interest (ROI_2) at the end of reperfusion, indicating less ischemia induced damage occurred in ROI_2 compared to that occurring in ROI_1 and ROI_3. After the onset of nitrogen breathing, a biphasic change in scattering power was observed, with an initial decrease in b, followed by a gradual increase. Observations from the current study indicate that in addition to significant changes in C_{HbO}, C_{HbR}, C_{HbT}, and StO_2 during hepatic ischemia, Monte Carlo simulation based multiple regression analysis demonstrates alterations in scattering power that are consistent with ischemia-induced changes in cellular and subcellular structures in hepatic tissue.

5. Discussion

In this paper, a model of light transport in tissue is applied to analyze the reflectance spectra of hepatic tissue following ischemia-reperfusion and post-mortem using an RGB imaging instrument. With the RGB imaging technique, it was possible to obtain images of oxyhemoglobin concentration, deoxyhemoglobin concentration, and scattering power. From these estimated images of oxyhemoglobin and deoxyhemoglobin concentrations, the images of total hemoglobin concentration and tissue oxygen saturation were reconstructed.

In the present study we examined the hemodynamic responses of rat liver during ischemia-reperfusion induced by portal triad occlusion. Here, we have demonstrated that 10 minutes of hepatic ischemia and 120 minutes of reperfusion are associated with disrupted hepatic blood flow with subsequent hemodynamic instability, which results in decreased C_{HbO}, C_{HbT}, and StO_2 during ischemia and reperfusion compared to baseline levels. We also observed that during a 120-min period of reperfusion there was a gradual increase in C_{HbO} and StO_2 along with a partial recovery of the initially severely depressed hepatic tissue, which is compatible with the hypothesis that no sinusoidal reflow occurs during the early stage of reperfusion, followed by subsequent reflow [33]. Changes in hepatic microvascular diameter

Biomedical Optics EXPRESS

during the early phase of reperfusion appear to be involved in post-ischemic reperfusion failure [33]. The major dysfunction of hepatic ischemia is the lack of re-establishment of nutritive blood flow, which causes hemoconcentration, including endothelial cell swelling, interstitial edema formation, and ultimately alters the microcirculation during reperfusion [34]. Microcirculatory dysfunction is characterized by heterogeneous perfusion of liver lobules observed during the early phase of reperfusion and involves extravasation of erythrocytes, and ultimately petechial bleeding [35].

The combination of a diverse architecture, large size, and low pressure gradient in liver predisposes the liver to heterogeneous perfusion of the hepatic vascular bed and distribution of portal blood to different portion of the liver lobes [36]. Furthermore, small differences in hydrostatic pressure could result in large imbalances in the flow of portal blood to different parts of the liver, at scales ranging from individual sinusoids to entire liver lobes leading to heterogeneity in perfusion [36]. Occlusion of both the hepatic artery and portal vein (Pringle maneuver) increased heterogeneity of perfusion compared to perfusion via the portal vein only [36] or the hepatic artery only [37]. However, we have not observed perfusion failure in entire liver lobules (shown in Fig. 4) following 10 minutes of portal triad occlusion, which is in contrast to studies of hepatic microcirculation after a longer period of ischemia (90 min) [38] and reperfusion (3 hours) [39]. The longer period of occlusion is characterized by a noticeable decrease in densely perfused sinusoids and is associated with an increased number of non-perfused liver lobules [39]. Longer periods of ischemia-reperfusion cause hepatocellular damage due to acute cellular injury at 3 to 6 hours of post reperfusion, including the onset of necrosis and apoptosis [39]. The prolongation of both ischemia and reperfusion periods may be the causative factor in the gradual suspension of sinusoids from perfusion, also called secondary sinusoidal perfusion failure [36], which ultimately yields a total microcirculatory shutdown of entire liver lobules.

Therefore, measurement of hepatic tissue oxygen saturation during the early phase of reperfusion is important to predict the degree of subsequent liver injury. Using RGB imaging of rat liver, we have demonstrated that the changes in hemodynamics in liver tissue correlate with the decreased C_{HbO} and StO_2 along with heterogeneous perfusion of the liver lobule, indicating the influence of nutritive perfusion deficiency in the manifestation of ischemia-reperfusion injury. Our results suggest that a decline in hepatic C_{HbO} and StO_2 after reperfusion, compared to the baseline level, is presumably involved in the mechanism of subsequent hepatocellular damage.

Furthermore, hepatic StO_2 and hepatic energy state could be reliable indicators of ischemia-reperfusion liver injury, especially for the diagnosis of early graft rejection following liver transplantation. The estimated hepatic tissue oxygen saturation depends primarily on hepatic blood flow, oxygen content of the hepatic artery and portal vein, and hepatic oxygen consumption [40]. The reduced reperfusion level of StO_2 reveals the disparity between oxygen supply and oxygen demand, as StO_2 is a function of the balance between hepatic oxygen supply and oxygen demand in hepatocytes. Moreover, oxygen demand in the initial stage of reperfusion was reported to be less than in the pre-ischemic period, due to impaired respiratory function of mitochondria in hepatocytes after ischemia-reflow process [41], which is indicated by decreased StO_2 levels during reperfusion. Decreases in oxygen supply and oxygen demand might occur during the initial stage of reperfusion, with the net effect resulting in insufficient oxygen supply being the dominant factor contributing to decreased C_{HbO} and StO_2, which in turn leads to regional liver hypoxia [3]. The disturbances in tissue oxygen saturation were simultaneously caused by an increase in C_{HbR} and a decrease in C_{HbO} due to hepatic inflow occlusion leading to a decrease in total hemoglobin concentration during ischemia. C_{HbT} started to increase on initiation of nitrogen breathing and reached its maximal level after respiratory arrest, revealing the occurrence of increased intrahepatic blood flow. The decreases in hepatic C_{HbO}, C_{HbT}, and StO_2 during ischemia observed herein were presumed to be largely due to temporary deterioration of hepatic blood

Biomedical Optics EXPRESS

supply, which then recovered gradually on subsequent reflow. With respect to the decreased hepatic blood flow, it has been reported that hepatic blood flow during the early stage of reperfusion is 30% to 75% of the initial values in an ischemic model [41]. Moreover, Clemens *et al*. [38] reported that the number of perfused sinusoids on the surface of liver lobes was decreased after ischemia and reperfusion, which is consistent with our findings that C_{HbO} and StO_2 remained lower than baseline values after reperfusion. While the exact mechanism related to the reduced C_{HbO} remains unclear, involvement of reperfusion injury might be responsible. It has been suggested that overproduction of toxic oxygen free radicals, followed by endothelial cell damage during reperfusion [42] and cell swelling due to ischemia results in altered hepatic blood flow [43]. Several mechanisms are proposed to contribute to post-ischemic reperfusion failure, including sinusoidal endothelial cell swelling with luminal narrowing, intracellular edema formation, and intravascular hemoconcentration [44]. Certain vasoactive substances released during reperfusion may lead to vasoconstriction of sinusoids in the liver, which results in microcirculatory disturbances. The microcirculatory alterations may induce local hypoxia in liver tissue, thereby resulting in liver damage. On the basis of our current findings, we conclude that hepatic hemoglobin concentrations and tissue oxygen saturation after initiation of reperfusion represent valuable indicators of later liver damage and serve as prognostic factors in clinical situations.

On the other hand, the significant decrease in scattering power during ischemia and immediately after the onset of nitrogen breathing is probably associated with depletion of mitochondrial energy production, leading to rounding and swelling of mitochondria, dilatation of the endoplasmic reticulum, and formation of plasma membrane protrusions called *blebs* [45]. Short periods of ischemia or anoxia are characterized by a rapid end to *bleb* formation upon reoxygenation [45], whereas hepatocyte vacuolation is more evident at 3-4 min after death under anoxic conditions [10,11].

The optical imaging system (using an RGB color camera) described in this manuscript has the ability to enable new insights into the spatiotemporal dynamics of hepatic function during ischemia-reperfusion. In addition to large hemodynamic changes in time course, such as those that occur during ischemia, the RGB camera can also image spatial changes in hemoglobin concentrations and tissue oxygen saturation during reperfusion. Thus, the RGB imaging technique may be useful in monitoring the hemodynamic responses of liver tissue resulting from the ischemia-reflow process. Multispectral imaging techniques have been widely used for extending diffuse reflectance spectroscopy to functional imaging of living biological tissues. Multispectral cameras give more spectral resolution than a digital RGB camera. Therefore, they could provide better results than with a digital RGB camera. On the other hand, a digital RGB camera is promising as a method of rapid and cost-effective imaging, which would be advantageous to practical uses in surgical microscope and laparoscope systems.

Since the mathematical analysis in the proposed method shown in Fig. 1 can be applied to a digital RGB camera, it will be available to analyze the same biological variables in other procedures where ischemia-reperfusion needs to be monitored such as liver plantation models [46,47]. We used cross-polarized light to reduce unnecessary specular reflection from the surface of liver tissue. Cross-polarized imaging could eliminate not only glare but also important information from the superficial region of liver tissue. Using both cross-polarized and parallel-polarized imaging could enhance the distribution of biological scatteres and morphological changes at the surface of the tissue [48]. We assumed a linear transformation to biological parameters from *XYZ*-values. It may be helpful to apply the matrix $\mathbf{N_2}$ with the higher order terms of *XYZ*-values instead of the current linear transformation when there is nonlinearity between biological parameters and *XYZ*-values. Those considerations should be investigated in future works.

Our data regarding the time courses in C_{HbO}, C_{HbR}, C_{HbT}, and StO_2 are in good accordance with the hemodynamics of liver tissue. The results of spatial and temporal changes in C_{HbO},

Biomedical Optics EXPRESS

C_{HbR}, C_{HbT}, StO_2, and b following ischemia and reperfusion demonstrated that our method is reliable and reproducible for evaluating hepatic hemodynamic parameters and tissue morphology. A notable association is found between the tissue oxygen saturation StO_2 measured using the RGB imaging technique and that measured using a reflectance fiber probe based diffuse reflectance spectroscopy [12,24], which supports the value of the RGB imaging technique in monitoring hepatic tissue perfusion and oxygenation.

6. Conclusions

In summary, we described a method that uses an RGB camera to visualize the hemodynamic consequences and tissue morphology of hepatic ischemia-reperfusion in exposed rat liver. By illuminating the surface of rat liver with a white LED, and recording the resultant RGB images, the images of hemodynamic parameters and scattering power b were reconstructed. We studied hepatic hemodynamic responses to ischemia-reperfusion to investigate the time course and spatial distribution of chromophore concentrations and tissue oxygenation. Our data support the view that hemodynamic changes in rat liver tissue under conditions of hepatic inflow occlusion resulted in ischemic changes in liver tissue followed by a subsequent recovery during reperfusion. Early reperfusion of liver tissue after 10-min of portal triad occlusion is characterized by heterogeneous perfusion of liver lobules with decreased oxygenated hemoglobin, whereas prolongation of the reperfusion period to two hours reduced the spatial inhomogeneity. The results of hepatic ischemia-reperfusion revealed spatial changes in hepatic hemodynamics, an increase in deoxyhemoglobin concentration, decreases in oxyhemoglobin concentration and tissue oxygen saturation during ischemia, which subsequently recovered on reperfusion. Time courses of changes in C_{HbO}, C_{HbR}, C_{HbT}, and StO_2 during hepatic inflow occlusion and on subsequent reflow are in agreement with the hemodynamic responses of hepatic ischemia-reperfusion. The results demonstrated that our imaging method could monitor changes in hemodynamic parameters resulting from hepatic inflow occlusion and could reflect the ischemia-reperfusion induced hepatic dysfunction after reperfusion. Moreover, time course of scattering power during ischemia-reperfusion and post-mortem indicate the occurrence of morphological changes in hepatic tissue such as swelling of mitochondria and hepatocyte vacuolation. As our method can detect ischemia and reperfusion successfully, we believe that simultaneous measurement of spatial and temporal changes in C_{HbO}, C_{HbR}, C_{HbT}, StO_2, and b has great potential for the diagnosis of tissue ischemia and reperfusion. This study shows the potential of RGB imaging to assess hepatic hemodynamics and morphological change as an indicator of hepatic tissue viability in liver transplantation.